Abstracta

Ano XXVI - N. 06

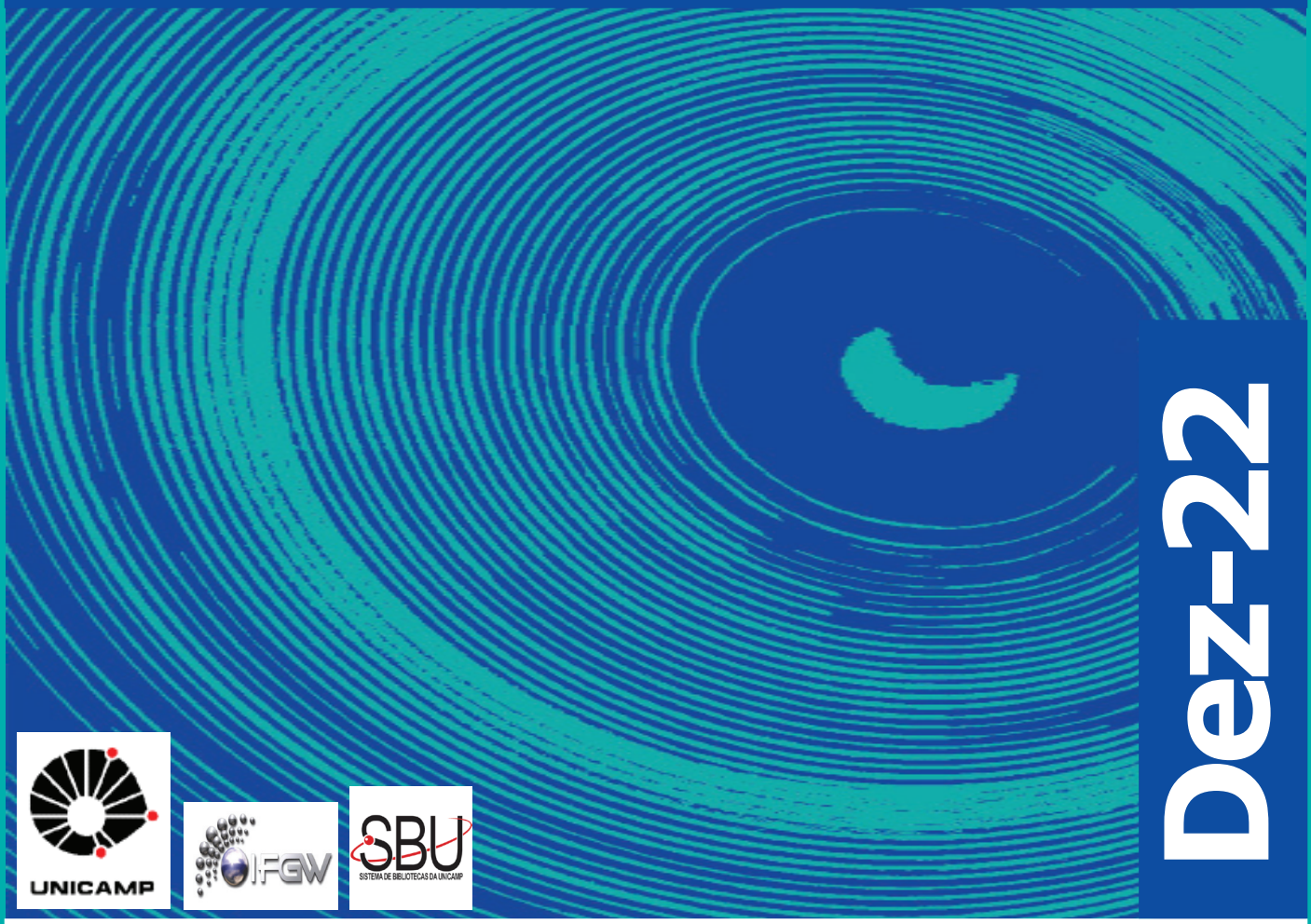

Dez-22

Artigos publicados - P254-2022 à P302-2022

Artigos de eventos - P303-2022 à P306-2022

Resumo de evento - R001-2022

Material editorial - M001-2022

Defesas de Dissertações do IFGW - D026-2022 à D027-2022

Defesas de Teses do IFGW - T023-2022 à T025-2022

Artigos publicados

[P254-2022] "A DFT study of the electronic, optical, and mechanical properties of a fullerene network"

Tromer, R. M.*; Junior, L. A. R.; **Galvao, D. S.***

Closely packed quasi-hexagonal and quasi-tetragonal crystalline phase of C(60)molecules (named qHPC(60)) was recently synthesized. Here, we used GGA-PBE based DFT simulations to investigate the optoelectronic and mechanical properties of qHPC(60) monolayers. qHPC(60) has a moderate direct electronic bandgap, with anisotropic mechanical properties. Their elastic modulus ranges between 50-62 GPa. The results for optical properties suggest that qHPC(60) can act as a UV collector for photon energies up to 5.5 eV since it presents low reflectivity and refractive index greater than one. The estimated optical bandgap (1.5-1.6 eV) is in very good agreement with the experimental one (1.6 eV).

CHEMICAL PHYSICS LETTERS 804, 139925, 2022. DOI: 10.1016/j.cplett.2022.139925

[P255-2022] "A tattoo-inspired electrosynthesized polypyrrole film: crossing the line toward a highly adherent film for biomedical implant applications"

Borges, M. H. R.; Nagay, B. E.; Costa, R. C.; Sacramento, C. M.; Ruiz, K. G.; **Landers, R.***; van den Beucken, J. J. J. P.; Fortulan, C. A.; Rangel, E. C.; da Cruz, N. C.; Barao, V. A. R.

Polypyrrole (PPy) films have demonstrated promising application for implants due to their unique topographical and electronic properties. However, the limited PPy adhesiveness to metallic surfaces remains a challenge. Consequently, we propose a two--step technique for the surface modification of titanium (Ti) via a plasma electrolytic oxidation (PEO) step to serve as mechanical interlocking for the subsequent deposition of a highly adherent PPy film (PEO thorn PPy). Ti discs with machined and PEO--modified surfaces were used as controls. For the experimental groups, PPy film was deposited onto such surfaces by electrodeposition. Then, the role of machined and PEO surfaces in the synthesis, con-ductivity, microstructure, mechanical, electrochemical, microbiological, and biological properties of the PPy film was investigated. The results showed that a highly adherent "tattoo-inspired" PPy thin film was successfully achieved when the Ti surface was pretreated via PEO. PEO thorn PPy enhanced Ti mechanical and tribological properties by inducing a lower friction coefficient and wear loss due to the cushion effect of PPy film, besides promoting higher corrosion resistance. The "cauliflower-like" morphology of the PPy favored protein adsorption, calcium phosphate growth and demonstrated cell biocompatibility. The as-sociation between PEO and PPy film can be considered bioactive and is promising for the triggering of superior long-term stability of biomedical implants.

MATERIALS TODAY CHEMISTRY 26, 101095, 2022. DOI: 10.1016/j.mtchem.2022.101095

[P256-2022] "An atomistic explanation of the ethanol-water azeotrope"

Carravetta, V.; **Gomes, A. H. de A.***; Marinho, R. dos R. T.; Ohrwall, G.; Agren, H.; Bjorneholm, O.; **Brito, A. N. de***

Ethanol and water form an azeotropic mixture at an ethanol molecular percentage of similar to 91% (similar to 96% by volume), which prohibits ethanol from being further purified via distillation. Aqueous solutions at different concentrations in ethanol have been studied both experimentally and theoretically. We performed cylindrical micro-jet photoelectron spectroscopy, excited by synchrotron radiation, 70 eV above C1s ionization threshold, providing optimal atomic-scale surface-probing. Large model systems have been employed to simulate, by molecular dynamics, slabs of the aqueous solutions and obtain an atomistic description of both bulk and surface regions. We show how the azeotropic behaviour results from an unexpected concentration-dependence of the surface composition. While ethanol strongly dominates the surface and water is almost completely depleted from the surface for most mixing ratios, the different intermolecular bonding patterns of the two components cause water to penetrate to the surface region at high ethanol concentrations. The addition of surface water increases its relative vapour pressure, giving rise to the azeotropic behaviour.

PHYSICAL CHEMISTRY CHEMICAL PHYSICS 24[42], 26037-26045, 2022. DOI: 10.1039/d2cp03145k

[P257-2022] "Analog model for the BTZ black hole"

Oliveira, C. C. de*; Mosna, R. A.

We present an analog model for the Banados, Teitelboim, Zanelli (BTZ) black hole based on a hydrodynamical flow. We numerically solve the fully nonlinear hydrodynamic equations of motion and observe the excitation and decay of the analog BTZ quasinormal modes in the process. We consider both a small perturbation in the steady state configuration of the fluid and a large perturbation; the latter could be regarded as an example of formation of the analog (acoustic) BTZ black hole.

PHYSICAL REVIEW D 106[6], 064030, 2022. DOI: 10.1103/PhysRevD.106.064030

[P258-2022] "Can tactile reactivity in preterm born infants be explained by an immature cortical response to tactile stimulation in the first year? A pilot study"

Machado, A. C. C. D.; Magalhaes, L. D.; Oliveira, S. R. de; **Novi, S. L.*; Mesquita, R. C. de*;** Miranda, D. M. de; Bouzada, M. C. F.

This study aimed to compare preterm (PT) and full-term (FT) infants' adaptive behavior and functional cortical response to tactile stimulus, as measured by Test of Sensory Functions in Infants and functional Near-Infrared Spectroscopy (fNIRS). Outcome measures were taken at 6 (PT = 26/FT = 21 infants) and 12 months (PT = 15/FT = 14 infants). At 6 months, poorer tactile reactivity was observed in PT, but not confirmed at 12 months. At 6 months, cortical response to tactile stimulus was found in the primary sensorimotor cortex and differences between groups did not reach significance. At 12 months, cortical response was found in the primary sensorimotor cortex and premotor area and in the somatosensory associative area, with significant less frequent response in premotor area in PT. The findings reinforce fNIRS as a tool to complement the knowledge of tactile adaptive behaviors in PT in early life.

JOURNAL OF PERINATOLOGY, 2022. DOI: 10.1038/s41372-022-01536-w. Acesso antecipado.

[P259-2022] "Cooling with cork: envisaging its giant compressive mechanocaloric effect for solid-state cooling devices"

Usuda, E. O.; Bocca, J. R.; **Paixao, L. S.***; Colman, F. C.; Radovanovic, E.; Fornazaro, G.; Carvalho, A. M. G.; Alves, C. S.; Favaro, S. L.

The urgent need for reducing greenhouse gasses leads to the search for better alternatives that do not compromise the environment.

Traditional refrigeration devices, for example, use harmful gasses as refrigerants and consume a lot of energy worldwide. Solid-state cooling devices based on mechanocaloric effects can be a better alternative that uses sustainable and eco-friendly materials with the potential to be more energy-efficient. Here, we study the compressive mechanocaloric effect in agglomerated cork: a natural, renewable, and sustainable material that has been used for centuries. We report giant values of entropy and temperature changes around room temperature, which peaks at the phase transition of suberin, a major component of cork. The results are promising and compete with the best mechanocaloric materials in the literature reported so far.

JOURNAL OF MATERIALS SCIENCE 57[37], 17700-17710, 2022. DOI: 10.1007/s10853-022-07749-w

[P260-2022] "Crystal-field Stark effect on the upconversion light emission spectrum of alpha-NaYF4 nanoparticles doped with Dy3+, Er3+, or Yb3+"

Garcia-Flores, A. F.*; Martinez, E. D.; Munevar, J.; Garcia, D. J.; Cornaglia, P. S.; **Fabris, F.*; Urbano, R. R.*; Rettori, C.***

NaYF4 nanoparticles (NPs) form in two crystal structures, cubic (alpha-phase) and hexagonal (beta-phase), each one presenting a different crystal electric field (CEF) Stark effect, that affects the upconversion (UC) light emission of the NPs when doped with rare-earth elements. Therefore, the knowledge of the CEF parameters, the wave functions, and energy levels of the rare earth (RE) J-multiplet is expected to be of great help for the understanding and improvement of the UC light emission. In this work, alpha-phase NaYF4 NPs doped with Dy3+, Er3+, or Yb3+ were investigated by means of magnetization, electron spin resonance (ESR), and optical spectroscopy techniques. Fittings of the temperature-and magnetic-field--dependent magnetization were performed to determine the fourth-and sixth-order cubic CEF parameters, B4 and B6. The ground state of Er3+, Yb3+, and Dy3+ in these alpha-NaYF4 NPs was confirmed by low-temperature ESR experiments. The obtained CEF parameters were used to write down a total Hamiltonian that allows to determine the CEF Stark splitting for all energy levels of the REs 4 f unfilled shell. We give details of how the Stark effect affects the overall energy splitting of the various J-multiplets and may explain the fine structure of the UC light emission in these cubic NaY1-delta RE delta F4 NPs.

PHYSICAL REVIEW B 106[12], 125427, 2022. DOI: 10.1103/PhysRevB.106.125427

[P261-2022] "Decoherence in the three-state quantum walk"

Tude, L. T.*; Oliveira, M. C. de*

Quantum walks are dynamic systems with a wide range of applications in quantum computation and quantum simulation of analog systems, therefore it is of common interest to understand what changes from an isolated process to one embedded in an environment. In the present work, we analyze the decoherence in a three-state uni-dimensional quantum walk. The approaches taken into consideration to account for the environment effects are phase and amplitude damping Kraus operators, unitary noise on the coin space, and broken links. The results are compared with the two-state quantum walk.

PHYSICA A-STATISTICAL MECHANICS AND ITS APPLICATIONS 605, 128012, 2022. DOI: 10.1016/j.physa.2022.128012

[P262-2022] "DFT-1/2 method applied to 3D topological insulators"

Mota, T.; **Matusalem, F.***; Marques, M.; Teles, L. K.; Guilhon, I.

In this paper, we present results and describe the methodology of application of DFT-1/2 method for five three-dimensional topological insulators materials that have been extensively studied in last years: Bi2Se3, Bi2Te3, Sb2Te3, CuTlSe2 and CuTlS2. There are many differences between the results of simple DFT calculations and quasiparticle energy correction methods for these materials, especially for band dispersion in the character band inversion region. The DFT-1/2 leads to quite accurate results not only for band gaps, but also for the shape and atomic character of the bands in the neighborhood of the inversion region as well as the topological invariants, essential quantities to describe the topological properties of materials. The methodology is efficient and ease to apply for the different approaches used to obtain the topological invariant Z (2), with the benefit of not increasing the computational cost in comparison with standard DFT, possibilitating its application for materials with a high number of atoms and complex systems.

JOURNAL OF PHYSICS-CONDENSED MATTER 34[46], 465501, 2022. DOI: 10.1088/1361-648X/ac8fd2

[P263-2022] "Disentangling X-Ray and Sunlight Irradiation Effects Under a Controllable Atmosphere in Metal Halide Perovskites"

Silva, F. M. C. da*; Szostak, R.; Teixeira, V. C.; Germino, J. C.; Soares, M. M.; Nogueira, A. F.; Tolentino, H. C. N.

Metal halide perovskites are versatile materials for photovoltaic and optoelectronic applications owing to their adjustable bandgap and emission properties. Nevertheless, a drawback is their photo-structural-chemical instability. Herein, structural and optical responses of metal halide perovskite films, exploiting in situ X-ray and visible light stimuli under dry and humid atmospheres, are correlated. It shows that the interplay of the physical parameters responsible for sample evolution depends in a nontrivial way on the nature of the excitation, radiation power density, and moisture conditions. Two perovskite samples demonstrate the relevance of each composition. They are resilient under a dry atmosphere, but the presence of water or oxygen molecules in the ambient air leads to structural and optical changes under irradiation. However, the sample reaction depends on the photons' excitation energy and power density to be effective. Under a dry atmosphere, the halide segregation involving Br and I atoms does not occur for the low-power density of X-ray and sunlight excitations. On the contrary, under the ambient air atmosphere, compound stability depends on sample composition, which relates to defects and traps, and the excitation source. Herein, the probe's relevance to perovskites' photoinduced structural and optical responses is highlighted.

SOLAR RRL, 2200898, 2022. DOI: 10.1002/solr.202200898, Acesso Antecipado

[P264-2022] "Electroluminescence of monolayer WS2 in a scanning tunneling microscope: Effect of bias polarity on spectral and angular distribution of emitted light"

Roman, R. J. P.*; Pommier, D.; Bretel, R.; Lopez, L. E. P.; Lorchat, E.; Chaste, J.; Ouerghi, A.; Le Moal, S.; Boer-Duchemin, E.; Dujardin, G.; Borisov, A. G.; **Zagonel, L. F.***; Schull, G.; Berciaud, S.; Le Moal, E.

Inelastic electron tunneling in a scanning tunneling microscope is used to generate excitons in monolayer tungsten disulfide (WS2). Excitonic electroluminescence is measured both at positive and negative sample bias. Using optical spectroscopy and Fourier-space optical microscopy, we show that the bias polarity of the tunnel junction determines the spectral and angular distribution of the emitted light.

At positive sample bias, only emission from excitonic species featuring an in-plane transition dipole moment is detected. Based on the spectral distribution of the emitted light, we infer that the dominant contribution is from charged excitons, i.e., trions. At negative sample bias, additional contributions from lower-energy excitonic species are evidenced in the emission spectra and the angular distribution of the emitted light reveals a mixed character of in-plane and out-of-plane transition dipole moments.

PHYSICAL REVIEW B 106[8], 085419, 2022. DOI: 10.1103/PhysRevB.106.085419

[P265-2022] "Enhanced Relative cooling Power and large inverse magnetocaloric effect of cobalt ferrite nanoparticles synthesized by auto-combustion method"

Hadouch, Y.; Mezzane, D.; Amjoud, M.; Hajji, L.; Gagou, Y.; Kutnjak, Z.; Laguta, V.; **Kopelevich, Y.***; El Marssi, M.

This work focuses on the microstructure, magnetic properties and magnetocaloric effect of CoFe2O4 (CFO) nanoparticles elaborated by the sol-gel auto combustion method. The XRD investigation indicates that CFO is crystallized in a cubic spinel structure with the Fd 3 m space group and the SEM micrograph shows fine quasi -spherical nanoparticles with an average grain size of 160 nm. The temperature dependence of the Raman spectra reveals the ferromagnetic to paramagnetic conversion started from 723 K. The magnetization temperature dependence reveals the Curie temperature at TC = 785 K. Large value of magnetocaloric temperature change of AT = 11.2 K with a high RCP of 687.56 J Kg-1 were measured indirectly via the Maxwell approach making our CFO nanopowder suitable candidate for both environmentally friendly magnetic refrigeration and medical ap-plications at ambient temperature.

JOURNAL OF MAGNETISM AND MAGNETIC MATERIALS 563, 169925, 2022. DOI: 10.1016/j.jmmm.2022.169925

[P266-2022] "Etching and optical properties of 1-2 MeV alpha particles irradiated CR-39 radiation detectors"

Pires, K. C. C.; Assuncao, M.; Rana, M. A.; **Guedes, S.***; Kunzel, R.; Trindade, N. M.

A comparison of track etch parameters at low energy alpha particles is presented, using the Lantrak and the Baryotrak CR-39 nuclear track detectors. Experimental data from literature, obtained through exposing CR-39 detectors at low energy alpha particles from a Am-241 source and, subsequently, etching them in NaOH, KOH, and NaOH+ethyl alcohol aqueous solutions at 70 degrees C and 80 degrees C, have been numerically analyzed here. Radial etch rates of alpha particle etch pits have been determined, compared, and critically discussed for both CR-39 types. Ratios of alpha etch pit diameters and etch pit densities have also been examined as a function of etching time, showing no notable differences in the comparison between these two detectors. This study has been extended from the structural point of view by performing new Ultraviolet-visible (UV-Vis) and Raman spectroscopy measurements on non-irradiated, alpha--irradiated and alpha-irradiated/etched Lantrak and Baryotrak detectors. The direct band-gap energies have been determined and no significant differences have been observed in detectors subjected to different conditions. The Raman spectra show that the CH2 functional group has been decreased when comparing the non-irradiated/alpha-irradiated and alpha-irradiated/etched detectors, suggesting a degradation of the detectors due to alpha particle irradiation and also due to the different chemical etching treatments applied. The uncertainties have been determined and reported along with the results.

NUCLEAR INSTRUMENTS & METHODS IN PHYSICS RESEARCH SECTION A-ACCELERATORS SPECTROMETERS DETECTORS AND ASSOCIATED EQUIPMENT 1041, 167370, 2022. DOI: 10.1016/j.nima.2022.167370

[P267-2022] "Ethanol in Aqueous Solution Studied by Microjet Photoelectron Spectroscopy and Theory"

Agren, H.; Bjorneholm, O.; Ohrwall, G.; Carravetta, V.; **Brito, A. N. de***

By combining results and analysis from cylindrical microjet photoelectron spectroscopy (cMJ-PES) and theoretical simulations, we unravel the microscopic properties of ethanol-water solutions with respect to structure and intermolecular bonding patterns following the full concentration scale from 0 to 100% ethanol content. In particular, we highlight the salient differences between bulk and surface. Like for the pure water and alcohol constituents, alcohol-water mixtures have attracted much interest in applications of X-ray spectroscopies owing to their potential of combining electronic and geometric structure probing. The water mixtures of the two simplest alcohols, methanol and ethanol, have generated particular attention due to their delicate hydrogen bonding networks that underlie their structural and thermodynamic properties. Macroscopically ethanol-water seems to mix very well, however microscopically this is not true. The aberrant thermodynamics of water-alcohol mixtures have been suggested to be caused by energy differences of hydrogen bonding between water-water, alcohol- alcohol and alcohol-water molecules. These networks may perturb the local character of the interaction between X-rays and matter, calling for analysis that go beyond the normally applied local selection and building block rules and that can combine the effects of light-matter, intra-and intermolecular interactions. However, despite decades of ongoing research there are still controversies of the precise nature of hydrogen bonding networks that underlie the mixing of these simple molecules. Our combined analysis indicates that at low concentration ethanol molecules form a film at the surface since ethanol at the surface can expose its hydrophobic part to the vacuum retaining its two (or three) possible hydrogen bonds, while water at the surface cannot retain all its four possible hydrogen bonds. Thus, ethanol at the surface becomes energetically favorable. Ethanol molecules show a tilting angle variation of the C-C axis with respect to the surface normal as large as 60 degrees at very low concentration. In bulk, around ca. ten %, the ethanol oxygen atoms tend to make a third acceptor hydrogen bond to water molecules. At ca. 20 %, there is a U-shaped change in the CH3 to CH2OH binding energy (BE) shift indicating the presence of ring-like agglomerates called clathrate structures. At the surface, between 5 and 25%, ethanol forms a closely packed layer with the smallest C-C tilting angle variation down to similar to 20 degrees. Above 25% and below the azeotrope at the surface, ethanol shows an increase in the tilting angle variation, while at very high ethanol concentrations water tends to move to the surface so giving a microscopic explanation of the azeotrope effect. This migration is connected to the presence of longer (shorter) ethanol chains in the bulk (surface). A brief comparison with discussions and predictions from other spectroscopic techniques is also given. We emphasize the execution of an integrated approach that combines molecular structural dynamics with quantum predictions of the core electronic chemical shift, so establishing a protocol with considerable interpretative as well as predictive power for cMJ-PES measurements. We believe that this protocol can valorize cMJPES for studies of properties of other alcohol mixtures as well as of binary solutions in general.

ACCOUNTS OF CHEMICAL RESEARCH 55[21], 3080-3087, 2022. DOI: 10.1021/acs.accounts.2c00471

[P268-2022] "Evaluation of the Reax Force-Field for Studying the Collision of an Energetic Proton with the DNA"

Faria, J. C. de*; Paupitz, R.; van Duin, A. C. T.; **Bernal, M. A.***

The early DNA damage induced by ionizing radiation depends on how ionizing particles transfer energy to this molecule and the surrounding medium, mostly water. In preliminary studies, we found that the energy transferred by a 4 keV proton to a cytosine- guanine base pair in a classical simulation collision using the ReaxFF potential is much smaller than that obtained by a quantum calculation using time-dependent density functional theory (TDDFT). We observed that there are two main reasons for that: no accurate force-field for this situation and problems while dealing with the proton charge during the collision. Here, we only focus on the interaction potential. We calibrated the van der Waals energy term of the ReaxFF potential using TDDFT calculations and a genetic algorithm, specifically for the interaction of a proton with the DNA constituent atoms (carbon, hydrogen, phosphorus, nitrogen, and oxygen). We obtained a significant improvement in the interaction potential and, consequently, in the scattering angle of the proton colliding with the target atoms in question. However, we conclude that despite the improvement for the force-field and scattering angle, the classical charge equilibration method should also be improved to properly describe the proton-DNA collision process.

JOURNAL OF CHEMICAL THEORY AND COMPUTATION 18[11], 6463-6471, 2022. DOI: 10.1021/acs.jctc2c00756.

[P269-2022] "Evidence of a glassy magnetic transition driven by structural disorder in BiFeO3 nanoparticles"

Rodriguez, A. C.; Reiber, A.; Schuller, I. K.; **Muraca, D.***; Ramirez, J. G.

Important effects appear in low and high temperature magnetometry of multiferroic BiFeO3 (BFO) nanoparticles as sizes are reduced from 105 nm to 18 nm. In these particles, a magnetic transition appears close to 200 K probably associated with a spin reorientation which is absent in bigger particles. At higher temperatures and up to the bulk ferroelectric Curie temperature (1000 K), two additional magnetic transitions can be identified. Around TN 600 K, a size-dependent magnetic transition appears, associated with an antiferromagnetic transition. A model based on atomic vibration instability can describe the variation of TN with nanoparticle size. Further-more, for certain sizes, the properties are dominated by the glassy state arising from the disorder produced by the formation of a core-shell structure. This implies that the magnetic behavior of nanoparticles is strongly affected by their crystal structure close to the transition temperature. The structural disorder which couples to the magnetic properties add control to the magnetic and ferroelectric properties of BFO nanoparticles.

JOURNAL OF MAGNETISM AND MAGNETIC MATERIALS 563, 169917, 2022. DOI: 10.1016/j.jmmm.2022.169917

[P270-2022] "Exploiting a future galactic supernova to probe neutrino magnetic moments"

Jana, S.; **Porto-Silva, Y. P.***; Sen, M.

A core-collapse supernova (SN) offers an excellent astrophysical laboratory to test non-zero neutrino magnetic moments. In particular, the neutronization burst phase, which lasts for a few tens of milliseconds post-bounce, is dominated by electron neutrinos and can offer exceptional discovery potential for transition magnetic moments. We simulate the neutrino spectra from the burst phase in forthcoming neutrino experiments like the Deep Underground Neutrino Experiment (DUNE), and the Hyper-Kamiokande (HK), by taking into account spin-flavour conversions of supernova neutrinos caused by interactions with ambient magnetic fields. We find that the sensitivities to neutrino transition magnetic moments which can be explored by these experiments for a galactic SN are an order to several orders of magnitude better than the current terrestrial and astrophysical limits. Additionally, we also discuss how this realization might provide light on three important neutrino properties: (a) the Dirac/Ma jorana nature, (b) the neutrino mass ordering, and (c) the neutrino mass-generation mechanism.

JOURNAL OF COSMOLOGY AND ASTROPARTICLE PHYSICS [9], 079, 2022. DOI: 10.1088/1475-7516/2022/09/079

[P271-2022] "First study of the two-body scattering involving charm hadrons"

Acharya, S.; Adamova, D.; **Albuquerque, D. S. D.*; Chinellato, D. D.*; Takahashi, J.***; et al. ALICE Collaboration

This article presents the first measurement of the interaction between charm hadrons and nucleons. The two-particle momentum correlations of pD(-) and (p) over barD(+) pairs are measured by the ALICE Collaboration in high-multiplicity pp collisions at root s = 13 TeV. The data are compatible with the Coulomb-only interaction hypothesis within (1.1-1.5) sigma. The level of agreement slightly improves if an attractive nucleon (N)(D) over bar strong interaction is considered, in contrast to most model predictions which suggest an overall repulsive interaction. This measurement allows for the first time an estimation of the 68% confidence level interval for the isospin I = 0 inverse scattering length of the N (D) over bar state f(0,I=0)(-1) is an element of[-0.4, 0.9] fm(-1), assuming negligible interaction for the isospin I = 1 channel.

PHYSICAL REVIEW D 106[5], 052010, 2022. DOI: 10.1103/PhysRevD.106.052010

[P272-2022] "Flat-band ferromagnetism in a correlated topological insulator on a honeycomb lattice"

Leite, L. S. G.*; Doretto, R. L.*

We study the flat-band ferromagnetic phase of a spinfull and time-reversal symmetric Haldane-Hubbard model on a honeycomb lattice within a bosonization formalism for flat-band Z2 topological insulators. Such a study extends our previous one [Phys. Rev. B 104, 155129 (2021)] concerning the flat-band ferromagnetic phase of a correlated Chern insulator described by a Haldane-Hubbard model. We consider the topological Hubbard model at 1/4 filling of its corresponding noninteracting limit and in the nearly flat band limit of its lower free -electronic bands. We define boson operators associated with two distinct spin-flip excitations, one that changes (mixed-lattice excitations) and a second one that preserves (same-lattice excitations) the index related to the two triangular sublattices. Within the bosonization scheme, the fermion model is mapped into an effective interacting boson model, whose quadratic term is considered at the harmonic approximation in order to determine the spin-wave spectrum. For both mixed-and same-lattice excitations, we find that the spin-wave spectrum is gapped and has two branches, with an energy gap between the lower and the upper bands at the K and K' points of the first Brillouin zone. We find that the same-lattice excitations are indeed the lowest-energy (elementary) excitations that characterize the flat-band ferromagnetic phase, a feature that contrasts with the behavior of a previously studied correlated topological insulator on a square lattice, whose flat-band ferromagnetic phase is characterized by mixed-lattice excitations. We also find some evidences that the spin-wave bands for the same-lattice excitations might be topologically nontrivial even in the completely flat band limit.

PHYSICAL REVIEW B 106[15], 155142, 2022. DOI: 10.1103/PhysRevB.106.155142

[P273-2022] "General balance functions of identified charged hadron pairs of (pi, K, p) in Pb-Pb collisions at root s(NN)=2.76 TeV"

Acharya, S.; Adamova, D.; **Chinellato, D. D.*; Guardiano, G. G.*; Jahnke, C.*; Takahashi, J.***; et al. ALICE Collaboration

First measurements of balance functions (BFs) of all combinations of identified charged hadron (pi, K, p) pairs in Pb-Pb collisions at root s(NN) = 2.76 TeV recorded by the ALICE detector are presented. The BF measurements are carried out as two-dimensional differential correlators versus the relative rapidity (Delta y) and azimuthal angle (Delta phi) of hadron pairs, and studied as a function of collision centrality. The Delta phi dependence of BFs is expected to be sensitive to the light quark diffusivity in the quark-gluon plasma. While the BF azimuthal widths of all pairs substantially decrease from peripheral to central collisions, the longitudinal widths exhibit mixed behaviors: BFs of pi pi and cross-species pairs narrow significantly in more central collisions, whereas those of KK and pp are found to be independent of collision centrality. This dichotomy is qualitatively consistent with the presence of strong radial flow effects and the existence of two stages of quark production in relativistic heavy-ion collisions. Finally, the first measurements of the collision centrality evolution of BF integrals are presented, with the observation that charge balancing fractions are nearly independent of collision centrality in Pb-Pb collisions. Overall, the results presented provide new and challenging constraints for theoretical models of hadron production and transport in relativistic heavy-ion collisions.

PHYSICS LETTERS B 833, 137338, 2022. DOI: 10.1016/j.physletb.2022.137338

[P274-2022] "Generation and transfer of entangled states between two connected microtoroidal cavities: Analysis of different types of coupling"

Sousa, E. H. S.*; Vidiella-Barranco, A.*; Roversi, J. A.*

We investigate the generation and transfer of entangled states between two coupled micro -toroidal cavities considering two different types of couplings, namely i) via a bridge qubit and ii) via evanescent fields. The cavities support two counter-propagating whispering-gallery modes (WGMs) that may also interact with each other. We firstly show that it is possible to transfer, with high fidelity, a maximally entangled state between the two modes of the first cavity (cavity 1) to the two modes of the second cavity (cavity 2), independently of the type of coupling. Interesting differences, though, arise concerning the generation of entangled states from initial product states; if the cavities are coupled via a bridge qubit, we show that it is possible to generate a 4-partite entangled state involving all four cavity modes. On the other hand, contrarily to what happens in the qubit coupling case, it is possible to generate bipartite maximally entangled states between modes of different cavities from initial separable states for cavities coupled by evanescent waves. Besides, we show that different entangled states between the propagating and counter-propagating modes of distinct cavities may be generated by tuning the interaction between modes belonging to the same cavity (intra-cavity couplings). Again, this is possible only for the couplings via evanescent waves. For the completion of our work, we discuss the effects of losses on the dynamics of the system.

OPTIK 271, 170016, 2022. DOI: 10.1016/j.ijleo.2022.170016

[P275-2022] "Guidelines for Engineering Directional Polariton Launchers"

Mayer, R. A.*; Feres, F. H.*; Maia, F. C. B.; Barcelos, I. D.; McLeod, A. S.; Rodin, A.; Freitas, R. O.

Nanophotonic devices based on two-dimensional crystals enable various technological applications, ranging from biosensing to quantum communication. In those devices, plasmonic antennas have been extensively explored in the photon--polariton conversion, as they allow field confinement within subdiffraction volumes. Despite the wide-reaching potential of polaritonics, essential rules for engineering polariton launchers are still to be developed, as the influence of the antenna geometry and source parameters on the polariton directivity is unknown. Here, we address this issue by combining concepts of radio-frequency antenna design with established polariton modeling. As an input for the model, we simulate hyperbolic phonon polariton waves in hexagonal boron nitride launched by metallic antennas. By adapting a Fresnel and Fraunhofer field regions formalism to polaritonics, we optimize the model accuracy and graphically represent several launching parameters as radiation patterns. Furthermore, we demonstrate how our framework can be applied to real antennas by employing it to experimental near-field images of polaritons reported in the literature. Our results show that the antenna geometry, its resonance order, and the angle of incidence of the light can strongly influence the polariton--wave pattern in the crystal. We foresee that our framework can add to further studies approaching optimized polariton launching and help the engineering of nanophotonic chips.

PHYSICAL REVIEW APPLIED 18[3], 034089, 2022. DOI: 10.1103/PhysRevApplied.18.034089

[P276-2022] "High oleic sunflower oil and fully hydrogenated soybean oil nanostructured lipid carriers: Development and characterization"

Ludtke, F. L.; Stahl, M. A.; Grimaldi, R.; **Cardoso, L. P.***; Gigante, M. L.; Ribeiro, A. P. B.

Lipid-based nanoparticles are among the most promising encapsulation technologies in the field of nanotech-nology. As one of the main trends in the development of these structures, the use of edible and/or commercially available oils and fats in the food industry stands out, replacing synthetic lipid matrices, which are not as viable for food applications in terms of cost, availability, or regulatory aspects. The objective of this work was to obtain and characterize nanostructured lipid carriers (NLC) using fully hydrogenated soybean oil (FHSO) and high oleic sunflower oil (HOSO) as lipid matrices. NLC were formulated from different lipid systems, 80:20, 60:40, 40:60, and 20:80 FHSO:HOSO (w/w), using soy lecithin (SL), Tween 80, or whey protein isolate (WPI) as an emulsifier. The increase in the unsaturation degree of the FHSO:HOSO lipid system resulted in larger NLC when obtained with Tween 80 or SL, greater physical instability, and lower peak temperature and melting enthalpy. The in-crease in the unsaturation degree, however, did not change the polymorphic shape of NLC, which stabilized in the beta form 48 h after their obtainment. Among the considered lipid systems, 80:20, 60:40, and 40:60 FHSO:HOSO (w/w) systems form stable particles, with crystallinity properties suitable for food incorporation.

COLLOIDS AND SURFACES A-PHYSICOCHEMICAL AND ENGINEERING ASPECTS 654, 130039, 2022. DOI: 10.1016/j.colsurfa.2022.130039

[P277-2022] "High performance of carbon nanotube elastocaloric refrigerators over a large temperature span"

Silva, T. N. Y.*; Fonseca, A. F.*

Compression of greenhouse gases still dominates the market of refrigeration devices. Although well es-tablished and efficient, this technology is neither safe for the environment nor able to be scaled down to nanoscale.

Solid-state cooling technologies are being developed to overcome these limitations, including studies at nanoscale. Among them, the so-called elastocaloric effect (eC) consists of the thermal response AT of a material under strain deformation. In this work, fully atomistic molecular dynamics simulations of the eC in carbon nanotubes (CNTs) are presented over a large temperature span. The efficiency of the CNTs as solid refrigerators is investigated by simulating their eC in a model of refrigerator machine running under Otto -like thermodynamic cycles (two adiabatic expansion/contraction plus two isostrain heat exchange processes) operating at temperatures TO ranging 300-2000 K. The coefficient of performance (COP), defined as the ratio of heat removed from the cold region to the total work performed by the system per thermodynamic cycle, is calculated for each value of TO. Our results show a nonlinear dependence of AT on TO, reaching a minimum value of about 30 K for TO between 500 and 600 K, then growing and converging to a linear dependence on TO for large temperatures. The COP of CNTs is shown to remain about the same and approximately equal to 8. These results are shown to be weakly depend on CNT diameter and chirality but not on length. The isothermal entropy change of the CNTs due to the eC is also estimated and shown to depend nonlinearly on TO values. These results predict that CNTs can be considered versatile nanoscale solid refrigerators able to efficiently work over a large temperature span.

PHYSICAL REVIEW B 106[16], 165413, 2022. DOI: 10.1103/PhysRevB.106.165413

[P278-2022] "Hollow-core photonic crystal fibers for Power--over-Fiber systems"

Osorio, J. H.*; Rosolem, J. B.; Bassan, F. R.; Amrani, F.; Gerome, F.; Benabid, F.; **Cordeiro, C. M. B.***

Research achievements in hollow-core photonic crystal fibers technology allow ascertaining such fibers as outstanding platforms for delivering high-power laser beams. Indeed, the key property underlying the success of this family of optical fibers for high-power beam delivery is their capability of efficiently transmitting light through empty space with minimal interaction with the fiber microstructure. In this context, here we widen the framework of hollow-core fiber-based beam delivery applications by demonstrating their utilization as promising platforms for Power-over-Fiber systems. Thus, we report on the use of a tubular-lattice hollow-core fiber to deliver a watt-level continuous-wave laser beam onto a photovoltaic converter and activate a representative camera circuit. We believe that the experiments reported herein allow identifying hollow-core fibers as eligible candidates for next-generation Power-over--Fiber devices potentially able to lift the power restrictions of current solid-core fiber-based Power-over-Fiber systems.

OPTICAL FIBER TECHNOLOGY 73, 103041, 2022. DOI: 10.1016/j.yofte.2022.103041

[P279-2022] "Identification of hadronic tau lepton decays using a deep neural network"

Tumasyan, A.; Adam, W.; **Chinellato, J. A.***; et al. CMS Collaboration

A new algorithm is presented to discriminate reconstructed hadronic decays of tau leptons (tau(h)) that originate from genuine tau leptons in the CMS detector against tau(h) candidates that originate from quark or gluon jets, electrons, or muons. The algorithm inputs information from all reconstructed particles in the vicinity of a tau(h) candidate and employs a deep neural network with convolutional layers to efficiently process the inputs. This algorithm leads to a significantly improved performance compared with the previously used one. For example, the efficiency for a genuine tau(h) to pass the discriminator against jets increases by 10-30% for a given efficiency for quark and gluon jets. Furthermore, a more efficient tau(h) reconstruction is introduced that incorporates additional hadronic decay modes. The superior performance of the new algorithm to discriminate against jets, electrons, and muons and the improved tau(h) reconstruction method are validated with LHC proton-proton collision data at root s = 13 TeV.

JOURNAL OF INSTRUMENTATION 17[7], P07023, 2022. DOI: 10.1088/1748-0221/17/07/P07023

[P280-2022] "Lead-Free Metal Halide Perovskite Nanocrystals: From Fundamentals to Applications"

Carvalho, T. A. D. de S.; Magalhaes, L. F.; Santos, C. I. D. do L.; Freitas, T. A. Z. de; **Vale, B. R. C.***; Fonseca, A. F. V. da ; Schiavon, M. A.

Lead (Pb) halide perovskite nanocrystals, with the general formula APbX(3), where A=CH3NH3+, CH(NH2)(2+), or Cs+ and X=Cl-, Br-, or I-, have emerged as a class of materials with promising properties due to their remarkable optical properties and solar cell performance. However, important issues still need to be addressed to enable practical applications of these materials, such as instability, mass production, and Pb toxicity. Recent studies have carried out the replacement of Pb by various less-toxic cations as Sn, Ge, Sb, and Bi. This variety of chemical compositions provide Pb-free perovskite and metal halide nanostructures with a wide spectral range, in addition to being considered less toxic, therefore having greater practical applicability. Highlighting the necessity to address and solve the toxicity problems related to Pb-containing perovskite, this review considers the prospects of the Pb-free perovskite, involving synthesis methods, and properties of them, including advantages, disadvantages, and applications.

CHEMISTRY-A EUROPEAN JOURNAL, e202202518, p. 1-18, 2022. DOI: 10.1002/chem.202202518

[P281-2022] "Low-Energy Electron Interactions with Resveratrol and Resorcinol: Anion States and Likely Dissociation Pathways"

Miranda, E. G. F. de; **Cornetta, L. M.***; Varella, M. T. do N.

We report a computational study of the anion states of the resveratrol (RV) and resorcinol (RS) molecules, also investigating dissociative electron attachment (DEA) pathways. RV has well--known beneficial effects in human health, and its antioxidant activity was previously associated with DEA reactions producing H2. Our calculations indicate a valence bound state (1*) and four resonances (2* to 5*) for that system. While the computed thermodynamic thresholds are compatible with DEA reactions producing H2 at 0 eV, the well-known mechanism involving vibrational Feshbach resonances built on a dipole bound state should not be present in RV. Our results suggest that the shallow 1* valence bound state is expected to account for H2 elimination, probably involving 1*/ *OH couplings along the vibration dynamics. The RS molecule is also an oxidant and a subunit of RV. Because two close-lying hydroxyl groups are found in the RS moiety, the H2-elimination reaction in RV should take place at the RS site. Our calculations point out a correspondence between the anion states of RV and RS and even between the thresholds. Nevertheless, the absence of bound anion states in RS, indicated by our calculations, is expected to suppress the H2-formation channel at 0 eV. One is led to conclude that the ethene and phenol subunits in RV stabilize the 1* state, thus switching on the DEA mechanism producing H2.

JOURNAL OF PHYSICAL CHEMISTRY A 126[42], 7667-7674, 2022. DOI: 10.1021/acs.jpca.2c05789

[P282-2022] "Magnetic resonance imaging texture analysis to differentiate ameloblastoma from odontogenic keratocyst"

Gomes, J. P. P.; Ogawa, C. M.; **Silveira, R. V.*; Castellano, G.***; Rosa, C. S. de; Yasuda, C. L.; Rocha, A. C.; Hasseus, B.; Orhan, K.; Braz-Silva, P. H.; Costa, A. L. F.

The differentiation between ameloblastoma (AB) and odontogenic keratocyst (OKC) is essential for the formulation of the surgical plan, especially considering the biological behavior of these two pathological entities. Therefore, developing means to increase the accuracy of the diagnostic process is extremely important for a safe treatment. The aim of this study was to use magnetic resonance imaging (MRI) based on texture analysis (TA) as an aid in differentiating AB from OKC. This study comprised 18 patients; eight patients with AB and ten with OKC. All diagnoses were determined through incisional biopsy and later through histological examination of the surgical specimen. MRI was performed using a 3 T scanner with a neurovascular coil according to a specific protocol. All images were exported to segmentation software in which the volume of interest (VOI) was determined by a radiologist, who was blind to the histopathological results. Next, the textural parameters were computed by using the MATLAB software. Spearman's correlation coefficient was used to assess the correlation between texture parameters and the selected variables. Differences in TA parameters were compared between AB and OKC by using the Mann-Whitney test. Mann-Whitney test showed a statistically significant difference between AB and OKC for the parameters entropy (P = 0.033) and sum average (P = 0.033). MRI texture analysis has the potential to discriminate between AB and OKC as a noninvasive method. MRI texture analysis can be an additional tool to differentiate ameloblastoma from odontogenic keratocyst.

SCIENTIFIC REPORTS 12[1], 20047, 2022. DOI: 10.1038/s41598-022-20802-7

[P283-2022] "Matrix coupling and generalized frustration in Kuramoto oscillators"

Buzanello, G. L.*; Barioni, A. E. D.*; Aguiar, M. A. M. de*

The Kuramoto model describes the synchronization of coupled oscillators that have different natural frequencies. Among the many generalizations of the original model, Kuramoto and Sakaguchi (KS) proposed a frustrated version that resulted in dynamic behavior of the order parameter, even when the average natural frequency of the oscillators is zero. Here, we consider a generalization of the frustrated KS model that exhibits new transitions to synchronization. The model is identical in form to the original Kuramoto model but written in terms of unit vectors and with the coupling constant replaced by a coupling matrix. The matrix breaks the rotational symmetry and forces the order parameter to point in the direction of the eigenvector with the highest eigenvalue, when the eigenvalues are real. For complex eigenvalues, the module of order parameter oscillates while it rotates around the unit circle, creating active states. We derive the complete phase diagram for the Lorentzian distribution of frequencies using the Ott-Antonsen ansatz. We also show that changing the average value of the natural frequencies leads to further phase transitions where the module of the order parameter goes from oscillatory to static.

CHAOS 32[9], 093130, 2022. DOI: 10.1063/5.0108672

[P284-2022] "Measurement of the Higgs boson width and evidence of its off-shell contributions to ZZ production"

Tumasyan, A.; Adam, W.; **Chinellato, J. A.***; et al. CMS Collaboration

Since the discovery of the Higgs boson in 2012, detailed studies of its properties have been ongoing. Besides its mass, its width-related to its lifetime-is an important parameter. One way to determine this quantity is to measure its off-shell production, where the Higgs boson mass is far away from its nominal value, and relating it to its on-shell production, where the mass is close to the nominal value. Here we report evidence for such off-shell contributions to the production cross-section of two Z bosons with data from the CMS experiment at the CERN Large Hadron Collider. We constrain the total rate of the off-shell Higgs boson contribution beyond the Z boson pair production threshold, relative to its standard model expectation, to the interval [0.0061, 2.0] at the 95% confidence level. The scenario with no off-shell contribution is excluded at a p-value of 0.0003 (3.6 standard deviations). We measure the width of the Higgs boson as Gamma(H) = 3.2(-1.7)(+2.4) MeV, in agreement with the standard model expectation of 4.1 MeV. In addition, we set constraints on anomalous Higgs boson couplings to W and Z boson pairs.

NATURE PHYSICS 18[11], 1329-+, 2022. DOI: 10.1038/s41567-022-01682-0

[P285-2022] "Mito-nuclear selection induces a trade-off between species ecological dominance and evolutionary lifespan"

Princepe, D.*; Aguiar, M. A. M. de*; Plotkin, J. B.

Mitochondrial and nuclear genomes must be co-adapted to ensure proper cellular respiration and energy production. Mito--nuclear incompatibility reduces individual fitness and induces hybrid infertility, which can drive reproductive barriers and speciation. Here, we develop a birth-death model for evolution in spatially extended populations under selection for mito--nuclear co-adaptation. Mating is constrained by physical and genetic proximity, and offspring inherit nuclear genomes from both parents, with recombination. The model predicts macroscopic patterns including a community's species diversity, species abundance distribution, speciation and extinction rates, as well as intraspecific and interspecific genetic variation. We explore how these long-term outcomes depend upon the parameters of reproduction: individual fitness governed by mito--nuclear compatibility, constraints on mating compatibility and ecological carrying capacity. We find that strong selection for mito-nuclear compatibility reduces the equilibrium number of species after a radiation, increasing species' abundances and simultaneously increasing both speciation and extinction rates. The negative correlation between species diversity and diversification rates in our model agrees with the broad empirical pattern of lower diversity and higher speciation/extinction rates in temperate regions, compared to the tropics. We conclude that these empirical patterns may be caused in part by latitudinal variation in metabolic demands and corresponding variation in selection for mito-nuclear function.

NATURE ECOLOGY & EVOLUTION 6, 1992-2002, 2022. DOI: 10.1038/s41559-022-01901-0

[P286-2022] "Mott domain walls: A (strongly) non-Fermi liquid state of matter"

Lee, T. H.; Vucicevic, J.; Tanaskovic, D.; **Miranda, E.***; Dobrosavljevic, V.

Most Mott systems display a low-temperature phase coexistence region around the metal-insulator transition. The domain walls separating the respective phases have very recently been observed displaying unusual properties both in simulations and in experiments. First, they often cover a significant volume fraction, thus cannot be neglected. Second, they resemble neither a typical metal nor a standard insulator, displaying unfamiliar temperature dependence of (local) transport properties.

Here we take a closer look at such domain wall matter by examining an appropriate unstable solution of the Hubbard model. We show that transport in this regime is dominated by the emergence of "resilient quasiparticles" displaying strong non-Fermi liquid features, reflecting the quantum--critical fluctuations in the vicinity of the Mott point.

PHYSICAL REVIEW B 106[16], L161102, 2022. DOI: 10.1103/PhysRevB.106.L161102

[P287-2022] "Nanotribology of Hydrogenated Amorphous Silicon: Sliding- Dependent Friction and Implications for Nanoelectromechanical Systems"

Leidens, L. M.; Michels, A. F.; Perotti, B. L.; **Alvarez, F.*; Zanatta, A. R.***; Figueroa, C. A.

Silicon-based materials are widely applied in micro-and nanoscale devices, such as micro-and nano-electromechanical systems (MEMs and NEMs, respectively). However, the nanofriction behavior of such materials is still an issue that influences or hinders some applications. Recently, a sliding-dependent friction mechanism was accessed, by simulation of hydrogenated silicon surfaces, in which friction forces increase during sliding. The experimental evaluation of this phenomenon is still lacking, as well as the confirmation of such a behavior in ambient air conditions, related to the current application. Here, the nanotribology of hydrogenated amorphous silicon (a--Si:H) was experimentally studied under repeated scanning. As an overall analysis, friction increases during sliding, without wear. After separation and new contact, the friction force recovers an intermediate value and increases again, until reaching an intermediate steady state. The mechanism may be related to the successive creation and breaking of bonds at the interface. When the contact is ceased, the dangling bonds created at both surfaces after separation may be repassivated. Moreover, the relationship of this behavior with the photoactivity of the material was tested. If an external light source is added during the scanning, it only changes the results before the stabilization of the interface. This detailed experimental study might promote the broader nanoapplication of the material, addressing the current failures and suggesting new devices based on the anomalous behavior.

ACS APPLIED NANO MATERIALS 5[10], 15546–15556, 2022. DOI: 10.1021/acsanm.2c03603

[P288-2022] "Neutral to charged kaon yield fluctuations in Pb - Pb collisions at , root S-NN=2.76 TeV"

Acharya, S.; Adamova, D.; **Chinellato, D. D.*; Guardiano, G. G.*; Jahnke, C.*; Takahashi, J.***; et al. ALICE Collaboration

We present the first measurement of event-by-event fluctuations in the kaon sector in Pb - Pb collisions at root S-NN = 2.76 TeV with the ALICE detector at the LHC. The robust fluctuation correlator nu(dyn) is used to evaluate the magnitude of fluctuations of the relative yields of neutral and charged kaons, as well as the relative yields of charged kaons, as a function of collision centrality and selected kinematic ranges. While the correlator nu(dyn) [K+,K-] exhibits a scaling approximately in inverse proportion of the charged particle multiplicity, nu(dyn) [K-S(0),K-+/-] features a significant deviation from such scaling. Within uncertainties, the value of nu(dyn) [K-S(0), K-+/-] is independent of the selected transverse momentum interval, while it exhibits a pseudorapidity dependence. The results are compared with HIJING, AMPT and EPOS-LHC predictions, and are further discussed in the context of the possible production of disoriented chiral condensates in central Pb - Pb collisions.

PHYSICS LETTERS B 832, 137242, 2022. DOI: 10.1016/j.physletb.2022.137242

[P289-2022] "Non-van der Waals quasi-2D materials; recent advances in synthesis, emergent properties and applications"

Balan, A. P.; Puthirath, A. B.; Roy, S.; Costin, G.; **Oliveira, E. F.*;** Saadi, M. A. S. R.; Sreepal, V.; Friedrich, R.; Serles, P.; Biswas, A.; Iyengar, S. A.; Chakingal, N.; Bhattacharyya, S.; Saju, S. K.; Pardo, S. C.; Sassi, L. M.; Filleter, T.; Krasheninnikov, A.; **Galvao, D. S.*;** Vajtai, R.; Nair, R. R.; Ajayan, P. M.

The discovery of novel materials that are stable at ambient conditions with emergent functionalities is a pressing need of the 21st century to keep the pace of social and technological advancement in a sustainable manner. Nanotechnology and nanomaterials are one of this kind and the current era has already witnessed several groundbreaking discoveries of materials and disruptive technological advancements. Starting from 0D fullerene, the invention of 1D carbon nanotubes, and most recently 2D graphene, all are allotropes of carbon, have brought a lot of research opportunities to understand different physical and chemical phenomena at atomic and molecular scales and to convert such properties into useful applications. Among them, 2D materials find special attention due to unique properties such as ballistic carrier transport, immunity from substrate effects and commendable in plane mechanical robustness. However, the library of such materials is limited, and one can see that most of the technically viable materials that are already industrialized in a large scale belong to the class of non-van der Waals materials. The effect of confinement in one dimension on non-van der Waals materials remains unexplored owing to the difficulty in fabricating these materials to the ultra-thin limit with large lateral size or area. Recent advancement of cleaving non-van der Waals bulk materials to their ultra-thin counter parts through the state--of-the-art liquid phase exfoliation approach leads to renewed research interest among scientific community. The existence of cleaving/-parting planes in certain directions of non-van der Waals materials, where the bonding strength is relatively weak compared to other crystallographic directions of the bulk crystal, facilitate smooth exfoliation when subjected to shear force through suitable methods. Herein, we attempt to discuss the rationale of such methods in the synthesis of non-van der Waals 2D materials that possess cleavage/parting planes with a special attention to natural ores, and to review the recent progress made in non-van der Waals two-dimensional materials with a special emphasis on emergent magnetism, catalysis, energy storage, and optoelectronics and related applications.

MATERIALS TODAY 58, 164-200, 2022. DOI: 10.1016/j.mattod.2022.07.007

[P290-2022] "On the Truncation of Series for the Electrical Current Flow in Rectangular Conducting Sheets"

Oliveira, F. S.*

This study deals with the simplification and the applicability of the van der Pauw method. The convergence analysis of the infinite series of sums that describe the electrical current flow in a rectangular sheet and its closed form based upon q-Pochhammer symbols are presented. Results from finite-element simulations show that the first term of the infinite series of sums is accurate enough for the experimental determination of the electrical resistivity in thin films, semiconductors, and low-dimensional systems.

BRAZILIAN JOURNAL OF PHYSICS 52[6], 206, 2022. DOI: 10.1007/s13538-022-01211-7

[P291-2022] "Physiochemically Distinct Surface Properties of SU-8 Polymer Modulate Bacterial Cell-Surface Holdfast and Colonization"

Anbumani, S.*; Silva, A. M. da*; Alaferdov, A.; **Santos, M. V. P. dos***; Carvalho, I. G. B.; Silva, M. de. S. e; Moshkalev, S.; Carvalho, H. F.; Souza, A. A. de; **Cotta, M. A.***

SU-8 polymer is an excellent platform for diverse applications due to its high aspect ratio of micro/nanostructure fabrication and exceptional physicochemical and biocompatible properties. Although SU-8 polymer has often been investigated for various biological applications, how its surface properties influence the interaction of bacterial cells with the substrate and its colonization is poorly understood. In this work, we tailor SU-8 nanoscale surface properties to investigate single-cell motility, adhesion, and successive colonization of phytopathogenic bacteria, Xylella fastidiosa. Different surface properties of SU-8 thin films have been prepared using photolithography processing and oxygen plasma treatment. A more significant density of carboxyl groups in hydrophilic plasma-treated SU-8 surfaces promotes faster cell motility in the earlier growth stage. The hydrophobic nature of pristine SU-8 surfaces shows no trackable bacterial motility and 5-10 times more single cells adhered to the surface than its plasma-treated counterpart. In addition, plasma-treated SU-8 samples suppressed bacterial adhesion, with surfaces showing less than 5% coverage. These results not only showcase that SU-8 surface properties can impact the spatiotemporal bacterial behavior but also provide insights into pathogens' prominent ability to evolve and adapt to different surface properties.

ACS APPLIED BIO MATERIALS 5[10], 4903-4912, 2022. DOI: 10.1021/acsabm.2c00632

[P292-2022] "Pressure-tuning of the electronic and magnetic properties of EuPt2Si2"

Reis, R. D. dos*; Veiga, L. S. I.*; Fabbris, G.; Garcia, F.; Haskel, D.; **Gandra, F. C. G.***; Souza-Neto, N. M.

Using the element and orbital selectivity of x-ray absorption spectroscopy at Eu and Pt L-3 edges we investigate the effects of the lattice contraction, induced by temperature and external pressure, on the magnetic and electronic properties of the EuPt2Si2 system. Our findings point to a clear relationship between the volume and the Eu valence in this material. From XANES experiments as a function of pressure we show that the Europium valence tends to stabilize at 3+ for pressures up to 27 GPa. The XMCD results demonstrate that pressure induced valence change of the Europium ion leads to a suppression of the magnetic ordering of the material. Altogether our results provide direct evidence that Eu-4f /5d electronic hybridization effects underlie the mechanism that regulates the valence and magnetic ordering in this material.

JOURNAL OF MAGNETISM AND MAGNETIC MATERIALS 560, 169619, 2022. DOI: 10.1016/j.jmmm.2022.169619

[P293-2022] "Scalable Synthesis and Characterization of Multilayer gamma-Graphyne, New Carbon Crystals with a Small Direct Band Gap'

Desyatkin, V. G.; Martin, W. B.; Aliev, A. E.; Chapman, N. E.; **Fonseca, A. F.*; Galvao, D. S.***; Miller, E. R.; Stone, K. H.; Wang, Z.; Zakhidov, D.; Limpoco, F. T.; Almahdali, S. R.; Parker, S. M.; Baughman, R. H.; Rodionov, V. O.

gamma-Graphyne is the most symmetric sp(2)/sp(1) allotrope of carbon, which can be viewed as graphene uniformly expanded through the insertion of two-carbon acetylenic units between all the aromatic rings. To date, synthesis of bulk gamma-graphyne has remained a challenge. We here report the synthesis of multilayer gamma-graphyne through crystallization-assisted irreversible cross-coupling polymerization. A comprehensive characterization of this new carbon phase is described, including synchrotron powder X-ray diffraction, electron diffraction, lateral force microscopy, Raman spectroscopy, infrared spectroscopy, and cyclic voltammetry. Experiments indicate that gamma-graphyne is a 0.48 eV band gap semiconductor, with a hexagonal a-axis spacing of 6.88 angstrom and an interlayer spacing of 3.48 angstrom, which is consistent with theoretical predictions. The observed crystal structure has an aperiodic sheet stacking. The material is thermally stable up to 240 degrees C but undergoes transformation at higher temperatures. While conventional 2D polymerization and reticular chemistry rely on error correction through reversibility, we demonstrate that a periodic covalent lattice can be synthesized under purely kinetic control. The reported methodology is scalable and inspires extension to other allotropes of the graphyne family.

JOURNAL OF THE AMERICAN CHEMICAL SOCIETY 144[39], 17999-18008, 2022. DOI: 10.1021/jacs.2c06583

[P294-2022] "Schwarzites and schwarzynes based load-bear resistant 3D printed hierarchical structures"

Oliveira, E. F.*; Ambekar, R. S.; **Galvao, D. S.***; Tiwary, C. S.

The unique topological features, such as complex and hierarchical porosity exhibited in nature have been the basis to create new materials and/or structures. Most studies have been focused on regular porous structures but hierarchical porous ones have not been yet fully investigated for stable structural designs. In this work, we have proposed and tested a new approach to create hierarchical porous structures, in which the mass density varies from the center to the borders, i.e, a radial gradient. To create these new structures we exploited the topology of two carbon-based families with different pore sizes, the schwarzites, and schwarzynes. We created fully atomistic models that were translated into macroscale ones that were then 3D printed. The mechanical behavior of the gradient structures was investigated by molecular dynamics simulations and mechanical compression tests of the printed models. Our results show that their mechanical response can be engineered (for instance, in terms of energy absorption, ballistic performance, etc.) and can outperform their corresponding density uniform structures.

ADDITIVE MANUFACTURING 60, 103180, Parte: A, 2022. DOI: 10.1016/j.addma.2022.103180

[P295-2022] "Schwinger-Dyson truncations in the all-soft limit: a case study"

Aguilar, A. C.*; Ferreira, M. N.; **Oliveira, B. M.***; Papavassiliou, J.

We study a special Schwinger-Dyson equation in the context of a pure SU(3) Yang-Mills theory, formulated in the background field method. Specifically, we consider the corresponding equation for the vertex that governs the interaction of two background gluons with a ghost-antighost pair. By virtue of the background gauge invariance, this vertex satisfies a naive Slavnov-Taylor identity, which is not deformed by the ghost sector of the theory. In the all-soft limit, where all momenta vanish, the form of this vertex may be obtained exactly from the corresponding Ward identity. This special result is subsequently reproduced at the level of the Schwinger-Dyson equation, by making extensive use of Taylor's theorem and exploiting a plethora of key relations, particular to the background field method. This information permits the determination of the error associated with two distinct truncation schemes, where the potential advantage from employing lattice data for the ghost dressing function is quantitatively assessed.

EUROPEAN PHYSICAL JOURNAL C 82[11], 1068, 2022. DOI: 10.1140/epjc/s10052-022-11034-0

[P296-2022] "Searches for Ultra-High-Energy Photons at the Pierre Auger Observatory"

Abreu, P.; Aglietta, M.; **Arbeletche, L. B.*; Chinellato, J. A.*; Franco, D. de O.*; Dobrigkeit, C.*; Fauth, A. C.*; Payeras, A. M***; et al. Pierre Auger Collaboration

The Pierre Auger Observatory, which is the largest air-shower experiment in the world, offers unprecedented exposure to neutral particles at the highest energies. Since the start of data collection more than 18 years ago, various searches for ultra-high-energy (UHE, E greater than or similar to 10(17) eV) photons have been performed, either for a diffuse flux of UHE photons, for point sources of UHE photons or for UHE photons associated with transient events such as gravitational wave events. In the present paper, we summarize these searches and review the current results obtained using the wealth of data collected by the Pierre Auger Observatory.

UNIVERSE 8[11], 579, 2022. DOI: 10.3390/universe8110579

[P297-2022] "Separation of track- and shower-like energy deposits in ProtoDUNE-SP using a convolutional neural network"

Abud, A. A.; Abi, B.; **Chagas, E. B. das*; Bazetto, M. C. Q.*; Holanda, P. C. de*; Souza, G. de*; Gelli, B.*; Giammaria, P.*; Guzzo, M. M.*; Kemp, E.*; Machado, A.*; Peres, O. L.*; Pimentel, V. L.*; Prakash, S.*; Segreto, E.***; et al. DUNE Collaboration

Liquid argon time projection chamber detector technology provides high spatial and calorimetric resolutions on the charged particles traversing liquid argon. As a result, the technology has been used in a number of recent neutrino experiments, and is the technology of choice for the Deep Underground Neutrino Experiment (DUNE). In order to perform high precision measurements of neutrinos in the detector, final state particles need to be effectively identified, and their energy accurately reconstructed. This article proposes an algorithm based on a convolutional neural network to perform the classification of energy deposits and reconstructed particles as track-like or arising from electromagnetic cascades. Results from testing the algorithm on experimental data from ProtoDUNE-SP, a prototype of the DUNE far detector, are presented. The network identifies track- and shower-like particles, as well as Michel electrons, with high efficiency. The performance of the algorithm is consistent between experimental data and simulation.

EUROPEAN PHYSICAL JOURNAL C 82[10], 903, 2022. DOI: 10.1140/epjc/s10052-022-10791-2

[P298-2022] "The Hubble constant troubled by dark matter in non-standard cosmologies"

Alcaniz, J. S.; **Neto, J. P.***; Queiroz, F. S.; Silva, D. R. da; **Silva, R.***

The Standard Cosmological Model has experienced tremendous success at reproducing observational data by assuming a universe dominated by a cosmological constant and dark matter in a flat geometry. However, several studies, based on local measurements, indicate that the universe is expanding too fast, in disagreement with the Cosmic Microwave Background. Taking into account combined data from CMB, Baryon Acoustic Oscillation, and type Ia Supernovae, we show that if the mechanism behind the production of dark matter particles has at least a small non-thermal origin, one can induce larger values of the Hubble rate H-0, within the Lambda CDM, to alleviate the trouble with H-0. In the presence of non-standard cosmology, however, we can fully reconcile CMB and local measurements and reach H-0 = 70-74 kms(-1) Mpc(-1).

SCIENTIFIC REPORTS 12[1], 20113, 2022. DOI: 10.1038/s41598-022-24608-5

[P299-2022] "The surface composition of amino acid - halide salt solutions is pH-dependent"

Gopakumar, G.; Unger, I.; Saak, C. M.; Ohrwall, G.; **Brito, A. N. de***; Rocha, T. C. R. da; Nicolas, C.; Caleman, C.; Bjorneholm, O.

In atmospheric aerosol particles, the chemical surface composition governs both heterogenous chemical reactions with gas-phase species and the ability to act as nuclei for cloud droplets. The pH in aerosol particles is expected to affect these properties, but it is very challenging to measure the pH in individual droplets, precluding the investigation of its influence on the particle's surface composition. In this work, we use photoelectron spectroscopy to explore how the surface composition of aqueous solutions containing inorganic salt and amino acids changes as a function of pH. We observe a change by a factor of 4-5 of the relative distribution of inorganic ions at the surface of a liquid water jet, as a function of solution pH and type of amino acid in the solution. The driving forces for the surface enhancement or depletion are ion pairing and the formation of charged layers close to the aqueous surface.

ENVIRONMENTAL SCIENCE-ATMOSPHERES 2[3], 441-448, 2022. DOI: 10.1039/d1ea00104c

[P300-2022] "Transport coefficients of quasiparticle models within a new relaxation time approximation of the Boltzmann equation"

Rocha, G. S.; **Ferreira, M. N.***; Denicol, G. S.; Noronha, J.

We investigate the transport properties of a kinetic theory model that is tuned to describe the thermodynamic properties of QCD at zero chemical potential using a new formulation of the relaxation time approximation. In contrast to previous approaches, the latter is constructed to preserve the fundamental properties of the collision term of the Boltzmann equation for any energy dependence of the relaxation time. A novel choice of matching conditions is implemented to ensure that the background mean-field depends only on the temperature even when the system is out of equilibrium. We provide a consistent analysis of how the transport coefficients of relativistic Navier-Stokes theory vary with the energy dependence of the relaxation time. We also show that the entropy production of this theory is consistent with the second law of thermodynamics and verify that it is independent of the matching conditions employed. We used this fact to calculate the matching independent combination of transport coefficients.

PHYSICAL REVIEW D 106[3], 036022, 2022. DOI: 10.1103/PhysRevD.106.036022

[P301-2022] "Type-II two-Higgs-doublet model in noncommutative geometry"

Jimenez, F.; **Restrepo, D.***; Rivera, A.

In noncommutative geometry (NCG) the spectral action principle predicts the standard model (SM) particle masses by constraining the scalar and Yukawa couplings at some heavy scale,

but gives an inconsistent value for the Higgs mass. Nevertheless, the scalar sector in the NCG approach to the standard model, is in general composed of two Higgs doublets and its phenomenology remains unexplored. In this work, we present a type-II two-Higgs-doublet model in NCG, with a SM-like Higgs mass compatible with the 125 GeV experimental value and extra scalars within the alignment limit without decoupling with masses from 350 GeV.

NUCLEAR PHYSICS B 983, 115923, 2022. DOI: 10.1016/j.nuclphysb.2022.115923

[P302-2022] "Vacancy-Mediated Anomalous Emission Characteristics of Size- Confined Semiconducting CoTe2"

Das, S.; Pal, S.; Kumbhakar, P.; **Tromer, R. M.***; Negedu, S. D.; **Galvao, D. S.***; Das, S.; Tiwary, C. S.; Ray, S. K.

Transition-metal tellurides (TMTs) are promising materials for "post-graphene age" nanoelectronics and energy storage applications owing to their industry-standard compatibility, high electron mobility, large spin-orbit coupling (SOC), etc. However, tellurium (Te) having a larger ionic radius (Z = 52) and broader d-bands endows TMTs with semimetallic nature, restricting their application in photonic and optoelectronic domains. In this work, we report the optical properties of the quantum-confined semiconducting phase of cobalt ditelluride (CoTe2) for the first time, exhibiting excellent two-color band photoabsorption attributes covering the UV-visible and near--infrared regions. Furthermore, novel excitonic resonances (X) of size-varying CoTe2 nanocrystals and quantum dots (QDs) are indicated by their temperature-dependent emission characteristics, which are attributed to the splitting of band edge states via confinement. On the other hand, the sudden rupture of the large-area CoTe2 nanosheets via ultrasonication incorporates Co vacancy-mediated localized trap states within the band gap, which is attributed to the superior room--temperature photoluminescence (PL) quantum yield of QDs and further corroborated using Raman analysis and atomistic density functional theory (DFT) simulations. Most interestingly, the excitonic peak of CoTe2 QDs reveals a unique positive-to--negative thermal quenching transition phenomenon, owing to the thermal activation of nonradiative surface trap states. These results introduce an exciting approach for the defect--mediated color-saturated light emission that paves the way for solution-processed telluride-based QD light-emitting diodes.

ACS APPLIED MATERIALS & INTERFACES 14[47], 53139-53149, 2022. DOI: 10.1021/acsami.2c14318

Artigos de eventos

[P303-2022] "Diagnostics of KB mirrors misalignment using Zernike rectangular polynomials and neural networks"

Luiz, S. A. L.*; Bueno, C. S. N. C.; **Silva, F. M. C.***; Celestre, R.; Meyer, B. C.; Oliveira, R. S.; **Tomal, A.***; **Tolentino, H. C. N.***; Dias, C. S. B.
Khounsary A. M.; Mimura H.; Morawe C. (Eds.)

The fine alignment of X-ray nano-focusing optics, such as Kirkpatrick-Baez (KB) mirrors, depends strongly on the ability to diagnose the X-ray beam at the focus position. Despite conventional diagnostics techniques (e.g. knife-edge) allowing the measurement of the beam profile with sub-micrometer resolution, they may yield poor accuracy for beams with sizes under 100 nm. With nanometer-resolution phase-recovering techniques like ptychography, information about optical aberrations can be obtained experimentally in the complex-valued wavefront. In this work, we use wave-propagation simulations with Synchrotron Radiation Workshop (SRW) to model the CARNAUBA beamline at Sirius. The beam phase at the KB mirrors exit pupil is decomposed in terms of Zernike rectangular polynomials. The relevant degrees of freedom (DOF) of the mirrors are scanned, allowing the correlation of the Zernike coefficients with the beam profile at focus. Therefore, the aberrations are classified and quantified for each mirror's DOF, and alignment tolerances are obtained. We find that each DOF can be described by a unique combination of only three Zernike terms. Additionally, a database with the first 15 Zernike coefficients is created by simulating random alignment states and used to train a simple fully-connected neural network. The neural network was able to determine the alignment states of unknown samples with errors below 3%. The combination of Zernike polynomials and neural networks could potentially lead to single-iteration alignment of KB mirrors using wavefront sensing techniques as a diagnostic tool.

ADVANCES IN X-RAY/EUV OPTICS AND COMPONENTS XVII, Série de livros: Proceedings of SPIE 12240, 1224003, 2022. DOI: 10.1117/12.2633614

[P304-2022] "Performance Comparison of Different Classifiers Applied to Gesture Recognition from sEMG Signals"

Sgambato, B. G.*; Castellano, G.*
Bastos-Filho T. F.; Caldeira E. M. D.; Frizera-Neto A. (Eds.)

In the last years, surface electromyography (sEMG) has become a hot spot for research on signal classification methods due to its many applications with consumer grade sensors. Nonetheless, the correct classification of sEMG signals is not simple due to their stochastic nature and high variability. Our objective was to provide a comprehensive comparison between schemes used on the latest research, namely convolution neural networks (CNN) and hyperdimensional computing (HDC) using a public high-quality dataset. Our results showed that while CNN had substantially higher accuracy (68 vs. 32% for HDC, for 18 gestures), its shortcomings may be more prevalent in this area, as low amounts of training data, and lack of subject specific data can cause an accuracy drop of up to 70%/19% and 56%/7% for CNN/HDC, respectively. Our results point out that while HDC cannot reach CNN classification levels it is more versatile on small datasets and provides more adaptability.

XXVII BRAZILIAN CONGRESS ON BIOMEDICAL ENGINEERING, CBEB 2020, Série de livros: IFMBE Proceedings, 1561-1568, 2022. DOI: 10.1007/978-3-030-70601-2_229

[P305-2022] "Single-Trial Functional Connectivity Dynamics of Event-Related Desynchronization for Motor Imagery EEG--Based Brain-Computer Interfaces"

Rodrigues, P. G.; **Fim-Neto, A.***; Sato, J. R.; Soriano, D. C.; Nasuto, S. J.
Bastos-Filho T. F.; Caldeira E. M. D.; Frizera-Neto A. (Eds.)

Functional connectivity (FC) analysis has been widely applied to the study of the brain functional organization under different conditions and pathologies providing compelling results. Recently, the investigation of FC in motor tasks has drawn the attention of researchers devoted to post-stroke rehabilitation and those seeking robust features for the design of brain-computer interfaces (BCIs). In particular, concerning this application, it is crucial to understand: (1) how motor imagery (MI) networks dynamics evolve over time; (2) how it can be suitably characterized by its topological quantifiers (graph metrics); (3) what is the discrimination capability of graph metrics for BCI purposes. This work aims to investigate the MI single-trial time-course of functional connectivity defined in terms of event-related desynchronization/ synchronization (ERD/S) similarity. Both ERD/S and clustering coefficient (CC) underlying FC were used as features for characterizing rest, right-hand MI, and left-hand MI for 21 subjects.

Our results showed that MI can be associated with a higher CC when compared to rest, while right- and left-hand MI present a similar CC time-course evolution. From the classification standpoint, ERD/S, CC and their combination provided moderate to substantial single electrode peak performances (in terms of Cohen's kappa) for discriminating rest and movement, i.e. for identifying alpha rhythm suppression. Weak peak classification performances were achieved for these features for right- and left-hand discrimination, but the combination of FC-based features and ERD/S provided significantly better results, suggesting complementary information. These results illustrate the symmetrical nature of brain activity relative power dynamics, as reflected in dynamics of functional connectivity during single trial MI and motivate need for further exploration of such measures for BCI applications.

XXVII BRAZILIAN CONGRESS ON BIOMEDICAL ENGINEERING, CBEB 2020, Série de livros: IFMBE Proceedings, 1887-1893, 2022. DOI: 10.1007/978-3-030-70601-2_275

[P306-2022] "Subthalamic Beta Burst Dynamics Differs for Parkinson's Disease Phenotypes"

Fim Neto, A.*; Luccas, J. B. de; Bianqueti, B. L.; Rocha, M. S.; Nasuto, S. J.; Godinho, F.; Soriano, D. C.
Bastos-Filho T. F.; Caldeira E. M. D.; Frizera-Neto A. (Eds.)

Resumo: Parkinson's Disease (PD) is a neurodegenerative illness associated with dopaminergic loss in the basal ganglia circuit which can lead to heterogeneous motor symptoms such as tremor, rigidity and bradykinesia. The electrophysiological phenomena underlying these symptoms is not completely understood, which imposes a major challenge for designing customized and more efficient Deep Brain Stimulation (DBS) protocols to match patients' specificities and needs. Recently, it has been shown that elevated and prolonged beta (13-35 Hz) oscillations (i.e. beta bursts) from the subthalamic nucleus (STN) are associated with motor impairment in PD. Furthermore, motor improvement induced by pharmacological treatment relates to attenuation of intermittent beta activity. This work aims to analyze beta burst dynamics of two phenotypes of PD patients-the tremor dominant (TD) and the postural instability and gait difficulty (PIGD)-to better understand how features of beta oscillations correlate with the motor symptoms in such different PD's categories. Through a wavelet analysis of 35 LFPs recorded in the sensorimotor portion of the STN from 15 TD and 20 PIGD patients, we show that PIGD patients exhibit longer beta bursts, while TD patients exhibit higher beta burst probability and an inverse significant correlation of burst duration with the rigidity score. These findings may provide critical markers for characterizing the electrophysiological mechanism underlying PD phenotypes and their symptoms, as also contribute to more efficient and customized DBS strategies.

XXVII BRAZILIAN CONGRESS ON BIOMEDICAL ENGINEERING, CBEB 2020, Série de livros: IFMBE Proceedings, 2219-2224, 2022 DOI: 10.1007/978-3-030-70601-2_325

***Autores da comunidade IFGW**
Fonte: Web of Science on-line (WOS)

Resumo de evento

[R001-2022] "Analysis of brain metabolism using FDG-PET/CT in patients with acute Covid-19"

Souza, S. de; Colet, N.; Fernandes, A.; Tobar, N.; Dertkigil, S.; **Takahashi, M.***; Amorim, B.; Yasuda, C.; Rodrigues, J.; Zantut-Wittmann, D.; Ramos, C.

EUROPEAN JOURNAL OF NUCLEAR MEDICINE AND MOLECULAR IMAGING OP-767 49[SUPPL 1], SI, S252-S252, Supl. 1, Sept. 2022

Material editorial

[M001-2022] "A Quantitative Experiment of Liquid Dispersion Using Merely a Partially Submerged Mirror and Sunlight"

Cordeiro, C. M. B.*; Fujiwara, E.*

PHYSICS TEACHER 60[2], 140-143, 2022. DOI: 10.1119/5.0022815

***Autores da comunidade IFGW**
Fonte: Web of Science on-line (WOS)

Defesas de Dissertações do IFGW

[D026-2022] "Infraestrutura de difração de raios X em alta resolução com pressão uniaxial"
Aluno: Vinícius Estevo Silva Frehse
Orientador: Prof. Dr. Ricardo Donizeth dos Reis
Data: 25/11/2022

[D027-2022] "Língua eletrônica microfluídica para análise de moléculas de doping e benzodiazepínicos"
Aluno: Maria Helena Gonçalves de Souza
Orientador: Prof. Dr. Varlei Rodrigues
Data: 14/12/2022

Defesas de Teses do IFGW

[T023-2022] "Um candidato à matéria escura no contexto da física além do modelo padrão"
Aluno: Guillermo Gerardo Rivera Gambini
Orientador: Prof. Dr. Pedro Cunha de Holanda
Data: 07/11/2022

[T024-2022] "Propriedades magnéticas e de transporte eletrônico em materiais magnéticos nanoestruturados"
Aluno: Murilo Ferreira Velo
Orientador: Prof. Dr. Kleber Roberto Pirota
Data: 07/12/2022

[T025-2022] "Oscilação paramétrica degenerada em moléculas fotônicas"
Aluno: Laís Fujii dos Santos
Orientador: Prof. Dr. Gustavo Silva Wiederhecker
Data: 20/12/2022

Fonte: Portal IFGW/Pós-graduação - Agenda de Colóquios, Defesas e Seminários.
Disponível em: http://portal.ifi.unicamp.br/pos-graduacao

Observação: Não ocorreram neste período defesas de teses e dissertações, com orientadores ou banca do IFGW, do Programa de Pós-Graduação Multiunidades em Ensino de Ciências e Matemática – Mestrado e Doutorado (PECIM) da Unicamp.
Fonte: Página do PECIM
Disponível em: https://www.pecim.unicamp.br/bancas

A BIF deseja a todos um Feziz Natal com muita paz e harmonia!

Abstracta

Instituto de Física
Diretora: Profa. Dra. Mônica Alonso Cotta
Diretor Associado: Prof. Dr. Marcos Cesar de Oliveira
Universidade Estadual de Campinas - UNICAMP
Cidade Universitária Zeferino Vaz
13083-859 - Campinas - SP - Brasil
e-mail: secdir@ifi.unicamp.br
Fone: +55 19 3521-5300

Publicação

Biblioteca do Instituto de Física Gleb Wataghin
http://portal.ifi.unicamp.br/biblioteca
Instagram: @bif.unicamp
Telegram: t.m/bifunicamp

Diretora Técnica: Sandra Maria Carlos Cartaxo
Coordenadora da Comissão de Biblioteca: Profa. Dra. Arlene Cristina Aguilar

Elaboração:
Maria Graciele Trevisan (Bibliotecária)
contato: infobif@ifi.unicamp.br